NJC

Accepted Manuscript

This is an *Accepted Manuscript*, which has been through the Royal Society of Chemistry peer review process and has been accepted for publication.

Accepted Manuscripts are published online shortly after acceptance, before technical editing, formatting and proof reading. Using this free service, authors can make their results available to the community, in citable form, before we publish the edited article. We will replace this *Accepted Manuscript* with the edited and formatted *Advance Article* as soon as it is available.

You can find more information about *Accepted Manuscripts* in the Information for Authors.

Please note that technical editing may introduce minor changes to the text and/or graphics, which may alter content. The journal's standard Terms & Conditions and the Ethical guidelines still apply. In no event shall the Royal Society of Chemistry be held responsible for any errors or omissions in this *Accepted Manuscript* or any consequences arising from the use of any information it contains.

ROYAL SOCIETY OF CHEMISTRY

www.rsc.org/njc

Cite this: DOI: 10.1039/c0xx00000x

www.rsc.org/xxxxxx

ARTICLE TYPE

Facile synthesized highly active BiOI/Zn_2GeO_4 composites for the elimination of endocrine disrupter BPA under visible light irradiation

Tao Yan[a,b], Hongye Liu[c], Picheng Gao[d], Meng Sun[a], Qin Wei[d], Wenguo Xu[b] Xiaodong Wang[c] and Bin Du*[a]*

Received (in XXX, XXX) XthXXXXXXXXX 20XX, Accepted Xth XXXXXXXXX 20XX

DOI: 10.1039/b000000x

Abstract: A simple chemical bath approach for facile synthesis of BiOI/Zn_2GeO_4 composite has been demonstrated. The as-prepared samples were characterized by X-ray diffraction (XRD), scanning electron Microscopy (SEM), transmission electron microscopy (TEM), high-resolution transmission electron microscopy (HRTEM), X-ray photoelectron spectroscopy (XPS), and UV-vis diffuse reflectance spectroscopy (UV-vis DRS). The XRD results indicate that the BiOI and Zn_2GeO_4 were co-existed in the composite. The HRTEM image showing clear lattice fringes proves the formation of heterojunction between BiOI and Zn_2GeO_4. The photo-degradations of bisphenol A indicated that the BiOI/Zn_2GeO_4 composites were more photoactive than BiOI and Zn_2GeO_4. The photocatalytic activity enhancement mainly ascribed to the strong sensitization of BiOI to Zn_2GeO_4 broadened the photoabsorption of Zn_2GeO_4, and the heterojunction of BiOI/Zn_2GeO_4 facilitated the transfer and separation of photo-generated charge carriers. In addition, the active species trapping experiments showed that h^+ and $\cdot O_2^-$ were the dominant reactive species, and the molecular oxygen play a fatal role for the photocatalytic interactions. Subsequently, a possible degradation mechanism is proposed. Furthermore, the BiOI/Zn_2GeO_4 photocatalysts exhibit higher mineralization capacity of bisphenol A, suggesting a hopeful prospect for the decomposition of organic pollutants in the practical application.

Keywords: BiOI/Zn_2GeO_4; Photocatalysis; Heterostructure; Visible light; BPA

Introduction

In recent years, concerns regarding the occurrence and treatment trials of Endocrine Disrupting Compounds (EDCs) have rapidly increased worldwide. Bisphenol A [2, 2-bis (4-hydroxyphenyl) propane, abbreviate BPA] is a typical endocrine disrupting compound, which may cause genital obstacles and various other adverse effects on variety of organisms [1-4]. BPA has already been listed as a priority pollutants in America, Japan and some European countries [5-6]. Due to its large consumption as an important intermediate in polymer materials and fine chemical production, such as polycarbonate, ethoxyline, plasticizers, antioxidants and pesticides [7-8], the elimination of BPA from the surface water has become a crucial environmental problem.

[a] *School of Resources and Environment, University of Jinan, Jinan 250022, P.R. China. Fax: +86 531 82765969; Tel: +86 531 82769235; E-mail: dubin61@gmail.com*

[b] *School of Chemistry, Beijing Institute of Technology, Beijing 100081, P.R. China. Fax: +86 10 68912631; Tel: +86 10 68913125; E-mail: xuwgujn@163.com*

[c] *School of Civil Engineering and Architecture, University of Jinan, Jinan 250022, P.R. China.*

[d] *Key Laboratory of Chemical Sensing & Analysis in Universities of Shan dong (University of Jinan), School of Chemistry and Chemical Engineering, University*

Recently, many physical [9], chemical [10], and biological [11, 12] technologies have been developed to remove BPA from water. Among these methods, photocatalytic degradation technology is attracting widespread concern due to its effective activity, low toxicity, and low energy consumption. Many studies have been reported on the degradation of BPA by photocatalysis [13-15].

Zn_2GeO_4 is an important ternary composite oxides that belongs to the photocatalytical active *p*-block metal oxide group with a d^{10} configuration [16]. Zn_2GeO_4 is demonstrated to be a prospective photocatalyst for the photodegradation of organic pollutants, water splitting, and carbon dioxide photo-reduction [17-18] due to its inherent feature such as electronic configuration, crystalline structure, and stability [19]. Unfortunately, Zn_2GeO_4 photocatalyst still cannot satisfy the requirements of practical application due to their poor photo-degradation ability and the limited ability of light absorption. Therefore, it is promising and inevitable to improve the photo-degradation efficiency of Zn_2GeO_4 by appropriate modification, such as doping, coupling, and supporting [20], which is necessary towards its practical applications in the environmental field.

As an efficient visible light driven photocatalyst, BiOI receives remarkable attentions in recent years, owing to its layered structures, the internal static electric field and the strong absorption in the visible light region. Especially, BiOI-based heterojunction photocatalysts usual present higher photocatalytic

activities than component phase alone, due to the formation of interface junction can facilitates the transfer and separation of photo-induced electron-hole pairs [21, 22]. As we all know, Several BiOI-based composites including BiOI/AgI [23], BiOI/TiO_2 [24], BiOI/ZnO [25], BiOI/$ZnTiO_3$ [26], and BiOI/Bi_2O_3 [27] etc. have been researched as visible light driven photocatalysts.

Herein, the BiOI/Zn_2GeO_4 composites were fabricated by a facile and straightforward chemical bath approach under mild conditions. The as-prepared composites exhibited excellent photocatalytic activity towards the decomposition of BPA under visible light irradiation. The experiment results suggested that the adoption of BiOI extend the response of Zn_2GeO_4 to visible light region, and the heterostructure of BiOI/Zn_2GeO_4 facilitates the transfer and separation efficiency of photo-generated electron-hole pairs, leading to the significantly enhancement of photo-degradation activity. The possible photocatalytic mechanism of BiOI/Zn_2GeO_4 heterostructure to BPA degradation were explored by adding sorts of radical scavengers in the photocatalytic system.

Experimental section

Synthesis of Zn_2GeO_4 nanorods

All chemicals with analytical purity were obtained from Sinopharm Chemical Reagent Co., Ltd and were used without further purification. Deionized water was employed in all experiments. The Zn_2GeO_4 nanorods were prepared using a solvothermal method reported previously with a little modification [28]. In a typical synthesis, 5 mM GeO_2 (0.52 g) and 10 mM $Zn(CH_3COO)_2{\cdot}2H_2O$ (2.19 g, molar ratio of Zn to Ge is 2:1) were added to 40 mL of solvents which includes 15 mL H_2O and 25 mL ethylenediamine (En). The mixture was stirred for 60 min and then transferred to a stainless Teflon-lined autoclave of 50 mL inner volume. After being stirred for 30 min, the solvothermal synthesis was performed under an auto-generated pressure at 180 ^oC for 24 h in an electric oven, followed by cooling to room temperature naturally. The product was collected by centrifugation, washed thoroughly with deionized water and alcohol several times, and then dried at 60 ^oC overnight. A white Zn_2GeO_4 powder was finally obtained and denoted as ZGO.

Preparation of BiOI/Zn_2GeO_4 composites

A measured amount of Zn_2GeO_4 was ultrasonically dispersed in 80 mL of distilled water to get a homogeneous solution. Then, different stoichiometric amounts of $Bi(NO_3)_3{\cdot}5H_2O$ and KI was dissolved in 10 mL ethylene glycol, respectively, and drop wise added to the above solution. On adding, cream pink-deep red precipitate was immediately formed. After being stirred for 60 min at room temperature, the system was refluxed at 80 °C for 2 h with vigorous stirring in an oil bath. The resulting precipitate was filtered, washed thoroughly with distilled water, and then dried at 60 °C for 12 h. The amounts of $Bi(NO_3)_3{\cdot}5H_2O$ and KI were varied to obtain BiOI/Zn_2GeO_4 composites with different mass ratios of BiOI/Zn_2GeO_4 at 20%, 25%, 30%, 35% and 40% were prepared and denoted as BiOI/ZGO-20, BiOI/ZGO-25, BiOI/ZGO-30, BiOI/ZGO-35 and BiOI/ZGO-40, respectively. PM-BiOI/ZGO-30 is the abbreviation for the BiOI/Zn_2GeO_4 composite prepared by physical mixing method with the same composition as BiOI/ZGO-30 (30 % BiOI and 70 % Zn_2GeO_4 powders physical mixed without any treatment). The neat BiOI was prepared by the same method without using Zn_2GeO_4 precursor. The N-doped TiO_2 (N-TiO_2) was prepared by the homogenous precipitation-solvothermal process in $TiCl_3$-HMT aqueous and methanol solution following with calcination at 400 ^oC for 4 h [29].

Characterization of photocatalysts

X-ray diffraction (XRD) patterns of the obtained products were recorded on a Bruker D8 Advance X-ray diffractometer under the conditions of generator voltage = 40 kV; generator current = 40 mA; divergence slit = 1.0 mm; Cu Kα (λ = 1.5406 Å); and polyethylene holder. Morphologies were characterized by a scanning electron microscopy (SEM) (Hitachi, S-3000N). Transmission electron microscopy (TEM) images and high-resolution transmission electron microscopy (HRTEM) images were obtained by a JEOL model JEM2010 EX instrument at the accelerating voltage of 200 kV. Carbon-coated copper grid was used as the sample holder. Energy-dispersive X-ray spectra (EDX) were obtained on a JEOL-2100 at an accelerating voltage of 200 kV. X-ray photoelectron spectroscopy (XPS) measurements were performed on a 2000 XPS system with a monochromatic Al Kα source and a charge neutralizer. UV–Vis diffuse reflectance spectrum (UV–Vis DRS) was recorded in the range of 200–700 nm on a Varian Cary 500 Scan UV–Vis–NIR spectrometer with BaSO4 as the background.

Photoelectrochemical measurements

The photoelectrochemical measurement was performed on CHI 760E electrochemical workstation (CHI 760E Chenhua Instrument Company, Shanghai, China) in a standard three-electrode system using the prepared samples as the working electrodes, a Pt wire as the counter electrode, and Ag/AgCl as a reference electrode. For the photocurrent measurement, A 300W Xe arc lamp through a UV–cutoff filter (λ > 420 nm) served as a light source, and 0.5 M Na_2SO_4 aqueous solution was used as the electrolyte. For the EIS measurement, 2.5 mM $K_3Fe(CN)_6/K_4Fe(CN)_6$ (1:1) mixture as redox probe in 0.1 M KCl solution with a frequency range from 0.1 Hz to 100 kHz at 0.5 V, and the amplitude of the applied sine wave potential in each case was 5 mV. The working electrodes were prepared as follows: An indium tin oxide (ITO) glass (2.0×1.0 cm) was cleaned thoroughly by acetone, ethanol, deionized water, and then dried in N_2 stream. Then, 5.0 mg of the ground sample was dispersed uniformly with 1.0 mL of distilled water and ultrasonic treatment 30 min, then 10 μL of above solution was added to surface of ITO and dried at 120 °C for 30 min.

Photocatalytic tests

Photocatalytic reactions were acted in a customized reactor with a cooling-water-cycle system maintaining the system temperature at 25 ºC. The visible light photocatalytic activity of BiOI/Zn_2GeO_4 composites were evaluated by photo-degradation of BPA in aqueous solution using a 300 W xenon lamp (PLS-SXE300C, Beijing Perfect Light Co. Ltd., Beijing) with a cutoff filter (λ > 420 nm) as light source. In each experiment, 100 mg of photocatalyst was added into 100 mL BPA solution (20 mg/L). Before irradiation, the suspensions were magnetically stirred in dark for 60 min to achieve an adsorption/desorption equilibrium.

At given time intervals, 3 mL of suspension was sampled and centrifuged to remove the photocatalyst. The resulting clear liquor was analyzed on a Persee UV−vis spectrophotometer (Model: TU 1810) to record the concentration changes of pollutant solution, Total organic carbon (TOC) was measured with an Elementar liqui TOC analyzer.

Results and discussion

In this work, BiOI/Zn_2GeO_4 composites with different weight ratios are prepared by simple chemical bath approach and are tested as photocatalysts in the photodegradation of BPA. The heterojunction of BiOI/Zn_2GeO_4 composite facilitates the transfer and separation of photo-generated charge carriers, which may lead to higher catalytic activity. Kinetic aspects of catalytic reaction, behavior of catalytic species, and mechanism of photo-degradation are described in this section.

Structural characterization

Figure 1 exhibits the XRD patterns of BiOI, Zn_2GeO_4, and BiOI/Zn_2GeO_4 composites. As we can see, all the characteristic peaks in Figure 1 could be indexed to the rhombohedral phase of Zn_2GeO_4 (JCPDS No.11-0687, Figure 1a) [28] and tetragonal phase BiOI (JCPDS No. 73-2062, Figure 1g) [30], respectively. The narrow and sharp peaks indicate high crystallinity of Zn_2GeO_4 and BiOI, and there was no detection of impurities. For the BiOI/Zn_2GeO_4 composites (Figure 1b-f), characteristic peaks for BiOI and Zn_2GeO_4 were both observed. Furthermore, with the increase of BiOI to Zn_2GeO_4 mass ratio, the peaks assigned to Zn_2GeO_4 became weaker which may cause by heterostructural formation between BiOI and Zn_2GeO_4, while that of BiOI became broader suggesting that the adoption of Zn_2GeO_4 could influence the crystal growth of BiOI [31].

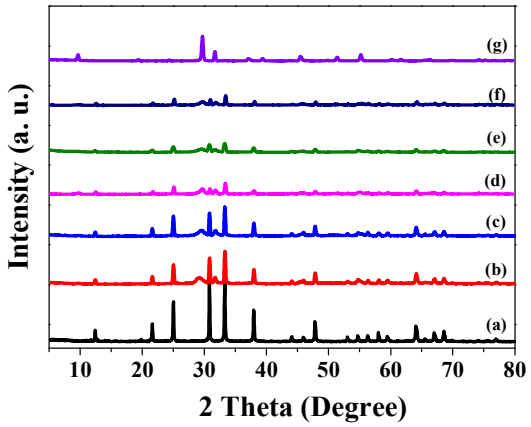

Figure. 1 XRD patterns of (a) pure Zn_2GeO_4, (b) BiOI/ZGO-20, (c) BiOI/ZGO-25, (d) BiOI/ZGO-30, (e) BiOI/ZGO-35, (f) BiOI/ZGO-40, and (g) pure BiOI.

The morphologies of Zn_2GeO_4, BiOI, and the BiOI/ZGO-30 composites have been characterized by SEM. As shown in Figure 2a-b, the pure BiOI showing uniquely layered structures, are composed of dozens of irregular plates with smooth surfaces, and the thickness of the plates are ~ 80 nm. The pure Zn_2GeO_4 presents irregular aggregates of nanorods with nouniform shapes (Figure 2c-d). As for the BiOI/ZGO-30 composite (Figure 2e-h), it can be seen that the Zn_2GeO_4 nanorods were coated entirely with the BiOI nanoflakes. By this means, the heterojunction interface between Zn_2GeO_4 and BiOI could be efficiently formed. During the deposition process, the Zn_2GeO_4 nanorods served as heterogeneous nuclei for the growth of BiOI, while the existence of Zn_2GeO_4 nanorods also inhibit the growing up of BiOI [31, 32], which is consistent with the above XRD analysis.

The formation of BiOI/Zn_2GeO_4 heterojunction was further confirmed by TEM and HRTEM. Figure 3a displays the typical TEM image of the BiOI/ZGO-30 composite. As we can see, the surface of the Zn_2GeO_4 are decorated with BiOI nanosheets, it was consistent with the SEM observations. Figure 3b presents the HRTEM image of the BiOI/Zn_2GeO_4 composite, the clear lattice fringes show that the as-prepared composites are highly crystallized. The lattice fringes of 0.29 nm and 0.71 nm corresponds to the (1 1 3) and (1 1 0) crystal plane of a rhombohedral structure of Zn_2GeO_4 [33], while the fringes of 0.30 nm and 0.20 matches well with the (1 0 2) and (1 1 3) plane of tetragonal phase BiOI [34]. Figure 3c presents the typical EDX mapping images, which indicates that the elements of Bi, O, I, Ge and Zn are uniformly distributed across the scanned distance. Figure 3d displays the EDX spectrum for the as-prepared composite. As we can see, only Bi, O, I, Ge and Zn elements existed in the as-prepared sample, implying that the composite was composed of both BiOI and Zn_2GeO_4.

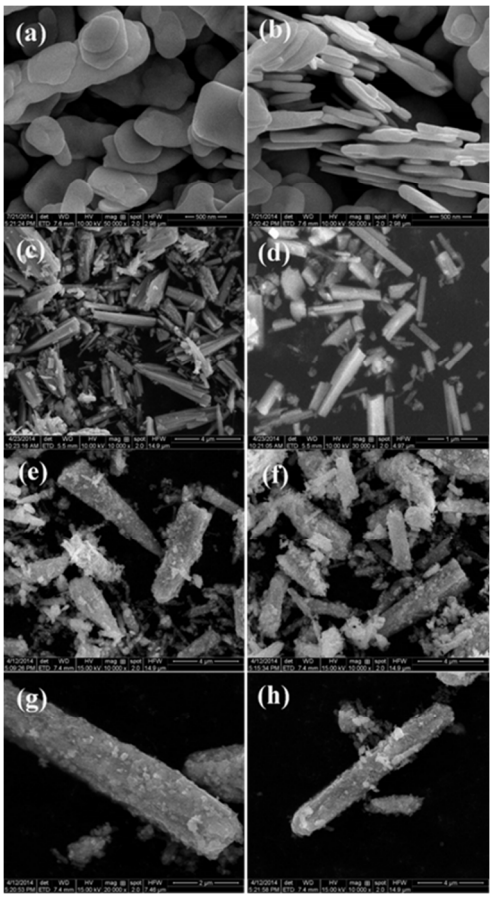

Figure. 2 SEM images of (a)-(b) BiOI, (c)-(d) Zn_2GeO_4, and (e)-(h) BiOI/ZGO-30.

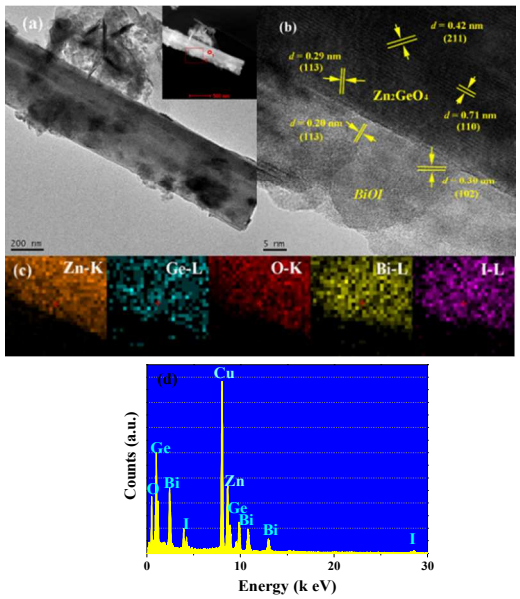

Figure 3. (a) TEM and (b) HRTEM image of BiOI/ZGO-30, (c) the corresponding mapping image of Zn, Ge, O, Bi and I elements, and (d) the EDX spectrum of BiOI/ZGO-30.

XPS spectra

The XPS spectra of Bi 4*f*, I 3*d* and O 1*s* for BiOI and BiOI/ZGO-30, as well as the Zn 2*p*, Ge 3*d* and O 1*s* spectra for Zn_2GeO_4 and BiOI/ZGO-30 are displayed in Figure 4. The electron binding energies were corrected for specimen charging by referencing the C 1*s* line to 284.6 eV. Figure 4a showed the survey scan XPS spectra for BiOI, Zn_2GeO_4 and BiOI/ZGO-30 composite, which was consistent with chemical composition of the photocatalysts.

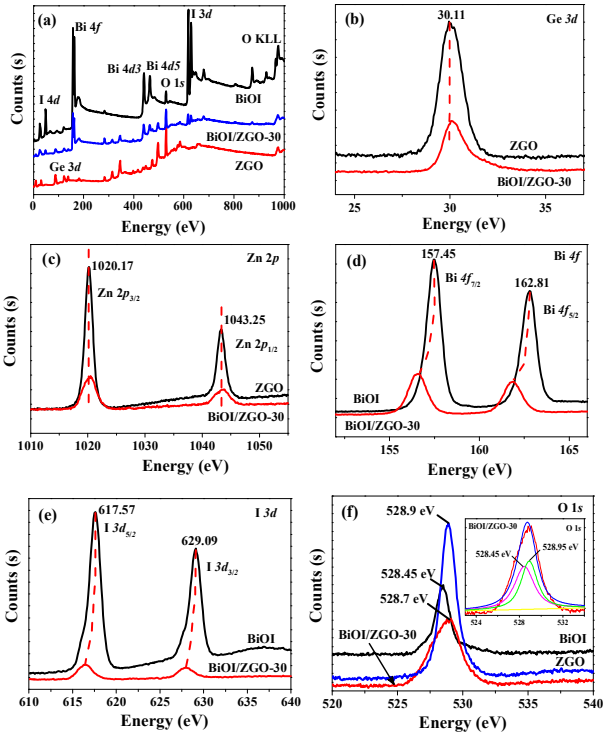

Figure 4. XPS spectra of Zn_2GeO_4, BiOI, and BiOI/ZGO-30, XPS spectra of (b) Ge 3d, (c) Zn 2p, (d) Bi 4f, (e) I 3d, and (f) O 1s peaks.

The carbon peak resulted from the adventitious carbon on the surface of the sample. Figure 4b-c shows the high resolution XPS spectra of Zn 2*p* and Ge 3*d* of the Zn_2GeO_4 and BiOI/ZGO-30. As we can see, the peaks at 1020.17, 1043.25 and 30.11 eV are attributed to Zn 2*p* (Zn $2p_{3/2}$ and Zn $2p_{1/2}$) (Figure 4b) and Ge 3*d* (Figure 4c) for the Zn_2GeO_4. However, compared with those of Zn_2GeO_4, the peaks of Zn 2*p* and Ge 3*d* of BiOI/ZGO-30 have a red-shift to the higher binding energy (about 0.50 eV and 0.30 eV). Figure 4d-e depicted the high resolution XPS spectra of Bi 4*f*, and I 3*d*. The two peaks located at 157.45 and 162.81 eV correspond to Bi 4*f* (Bi $4f_{7/2}$ and Bi $4f_{5/2}$) (Figure 4d). The peaks located at 617.57 and 629.09 eV are assigned to I 3*d* (I $3d_{5/2}$ and I $3d_{3/2}$) (Figure 4e). The Bi 4*f* peaks for BiOI/ZGO-30 have a blue-shift toward the lower binding energy (~ 1.00 eV) compared with these of pure BiOI. Besides, the I 3*d* (I $3d_{5/2}$ and I $3d_{3/2}$) peaks also transfers to the lower binding energy region (Figure 4e). Figure 4f exhibits the spectra of O1*s* for BiOI, Zn_2GeO_4 and BiOI/ZGO-30. The photoelectron peak of O 1*s* curve for BiOI/ZGO-30 is dissymmetrical and divides into two peaks (shown in Figure 4f inset). As we can see, the peaks at 528.45 eV and 528.95 eV are characteristic of O^{2-} in Zn_2GeO_4 and BiOI, respectively. The shift of the electron binding energy could be ascribed to the interaction between BiOI and Zn_2GeO_4, which possess different electronegativity, resulting in the shift of valence electrons and the change of electric screening of inner shells. The XPS results indicate the existence of electron transfer process and chemical bonds effect between BiOI and Zn_2GeO_4 in the heterojunctions.

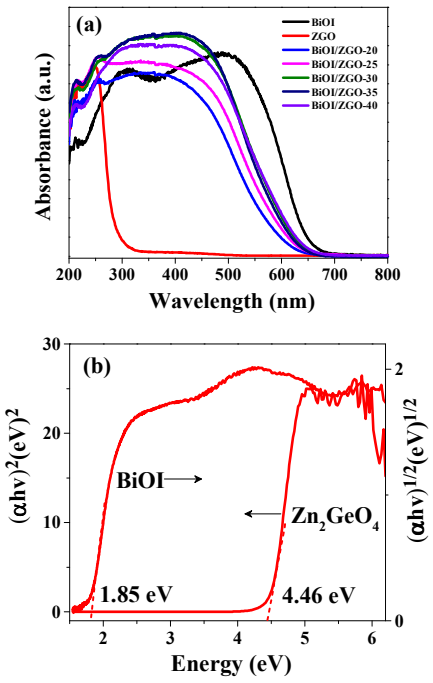

Figure 5. (a) UV–vis DRS of Zn_2GeO_4, BiOI and BiOI/Zn_2GeO_4 composites, (b) plots of $(ahv)^{n/2}$ versus photon energy (hv) for the band gap energies of BiOI and Zn_2GeO_4.

Optical characterization

The UV-vis DRS of the as-prepared BiOI/Zn_2GeO_4 composites are shown in Figure 5a. The absorption edge of Zn_2GeO_4 was

estimated to 275 nm showing a strong absorption in the UV range, and that of BiOI was estimated to 675 nm presenting an intense absorption in a wide wavelength range. However, When Zn_2GeO_4 combines with different amounts of BiOI, the optical absorption edge shift to longer wavelength region comparison that of Zn_2GeO_4, indicating the addition of BiOI has a narrowing effect on the band gap of the composite. The band gap energy of a semiconductor can be estimated by using the following equation [35]:

$$ahv = A\,(hv - E_g)^{n/2}$$

where a is the absorption coefficient, h is Plank constant, v is light frequency, A is a constant, E_g is band gap energy of the semiconductor, and n depends on the type of transition: $n = 1$ for a direct band transition, and $n = 4$ for an indirect band transition. For Zn_2GeO_4 and BiOI, the calculated values of n are 1 and 4 [36, 37], respectively. Therefore, the band gap energies of the BiOI and Zn_2GeO_4 can be calculated from the plots of $(\alpha hv)^2$ or $(\alpha hv)^{1/2}$ versus photon energy (hv), respectively. Figure 5b shows that the calculated band gaps (E_g) of Zn_2GeO_4 and BiOI is 4.46 and 1.85 eV, respectively. In addition, the band edge positions of Zn_2GeO_4 and BiOI were calculated according to the concept of electronegativity. The conduction band (CB) and valence band (VB) potentials are estimated by the following equations [38]:

$$E_{VB} = X - E_c + 0.5E_g$$

$$E_{CB} = E_{VB} - E_g$$

where E_{VB} is the VB edge potential, E_{CB} is the CB edge potential, X is the electronegativity of the semiconductor, which is the geometric mean of the electronegativity of the constituent atoms, the X values for Zn_2GeO_4 and BiOI were calculated to be 6.05 eV and 5.94 eV [38, 39], respectively. E_c is the energy of free electrons on the hydrogen scale (~ 4.5 eV), E_g is the band gap energy of the semiconductor. Correspondingly, the VB and CB of Zn_2GeO_4 were estimated to be +3.78 and −0.68 eV (*vs*. NHE), respectively. Likewise, the VB and CB of BiOI were calculated to be +2.42 and +0.57 eV (*vs*. NHE), respectively.

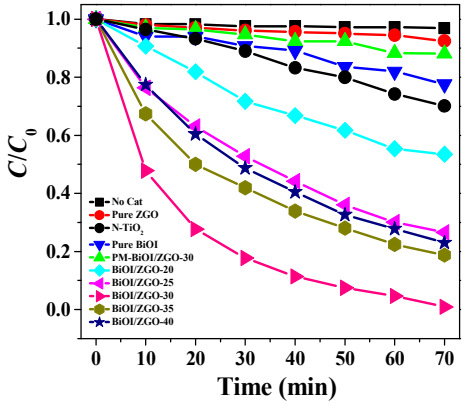

Figure 6. Photocatalytic activities of Zn_2GeO_4, BiOI, BiOI/Zn_2GeO_4 composites and N-TiO_2 for the degradation of BPA (20 mg/L) under visible light ($\lambda > 420$ nm) irradiation.

Photocatalytic activity

The photo-degradation performance of BiOI, Zn_2GeO_4, and BiOI/Zn_2GeO_4 composites were performed towards the degradation of BPA in water under visible light (λ>420 nm) illumination. Figure 6 displays the photo-degradation curve of

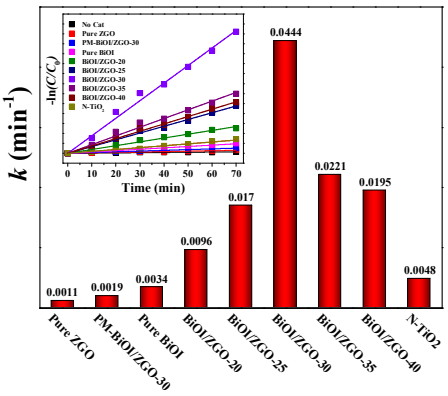

Figure 7. Comparison of photocatalytic degradation rate constant k of BiOI, Zn_2GeO_4, BiOI/Zn_2GeO_4 composites and N-TiO_2 for the degradation of BPA.

BPA over the BiOI, Zn_2GeO_4, and BiOI/Zn_2GeO_4 composites. For comparison purposes, we also conducted the blank experiments of BPA direct photolysis and BPA photo-degradation over PM-BiOI/ZGO-30 and N-TiO_2 under identical conditions. No obvious degradation of BPA was observed in the blank of photocatalyst or when using pure Zn_2GeO_4 as photocatalyst. Figure 7 describes the corresponding first-order kinetics curves by the formula of $\ln(C/C_0) = -kt$, where C_0 and C are the BPA concentrations at illumination times 0 and t, respectively, and k is the apparent rate constant. As we can see, pure Zn_2GeO_4 shows a low photo-degradation activity, and the photo-degradation rate is 0.0011 min^{-1}. Similarly, the pure BiOI also exhibits a low BPA photo-degradation rate of 0.0034 min^{-1}. With increasing of BiOI mass ratio, the photo-degradation rate of BPA over BiOI/Zn_2GeO_4 composites first rise and then drop. The composite with 30 % BiOI/Zn_2GeO_4 (BiOI/ZGO-30) content presents the highest photocatalytic activity, and the corresponding rate constant k is 0.0444 min^{-1}, which is 40 and 13 times higher than that of Zn_2GeO_4 and BiOI, respectively. These results indicated that the promotion of photo-degradation capacity could be attributed the synergetic effects of heterojunction and light absorption range of the resultant composite. Concretely, the light absorption region of BiOI/Zn_2GeO_4 composite broaden and generated more photo-induced carriers as the content of BiOI increasing, resulting more heterojunction interface could be formed between BiOI and Zn_2GeO_4, which facilitating the effective transfer and separation of photo-induced carriers. Inversely, when the BiOI mass ratio beyond the optimal condition, the heterogeneous interface would not increase efficiently, and thereby the redundant BiOI would be served as the recombination center, resulting the separation efficiency of photo-induced carriers reduced and restraining the photocatalytic activity of the photocatalyst. Furthermore, the performances of PM-BiOI/ZGO-30 and N-TiO_2 towards BPA photo-degradation were obviously lower than all that of BiOI/Zn_2GeO_4 composites, further confirmed that the heterojunction efficient promoted the separation and transfer of photo-induced electron-hole pairs.

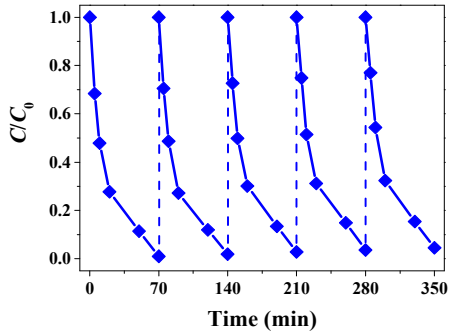

Figure 8. Recycling test on BiOI/ZGO-30 for the degradation of BPA under visible light irradiation.

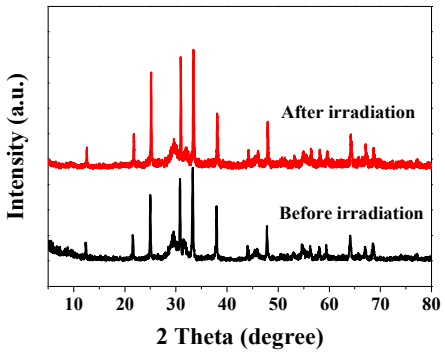

Figure 9. XRD patterns of the BiOI/ZGO-30 composite before and after visible light irradiation.

Regeneration and reusability

The stability of BiOI/Zn_2GeO_4 composite was assessed by recycling the photocatalyst and repeating the photo-degradation experiment for five times. After every circulation of photocatalytic experiment, the photocatalyst was separated by centrifugal and washed with deionized water and dried in 60 °C. The cyclic experiment results are showed in Figure 8. As we can see, the photocatalytic ability of BiOI/ZGO-30 composite towards BPA decomposition dropped slightly compared with the fresh photocatalyst. The XRD results further confirmed that the phase structure of BiOI/ZGO-30 composite did not change after the photocatalytic process (see Figure 9). It is apparent could be induces that the BiOI/Zn_2GeO_4 composite is stable, maintaining the photocatalytic activity for over five reaction cycles.

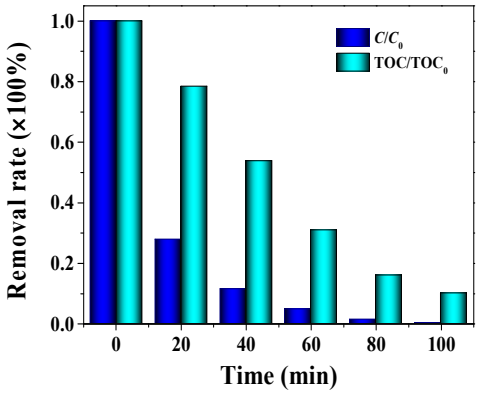

Figure 10. Temporal concentration change of BPA and TOC removal in the presence of BiOI/ZGO-30 (BPA concentration: 20 mg/L, catalyst dosage: 1.0 g L^{-1}, neutral condition).

TOC monitoring

In order to evaluate the photocatalytic performance of BiOI/Zn_2GeO_4 composite to completely decompose organic molecules in aqueous solution, total organic carbon (TOC) was monitored during the photodegradation process. As shown in Figure 10, about 50 % of TOC was removed from the reaction system after 40 min reaction with BiOI/ZGO-30 as photocatalyst under visible light irradiation while about 90% was removed in 100 min. These results indicated that the photodegradation of BPA by BiOI/ZGO-30 displayed an outstanding advantage in mineralization organics to CO_2 and H_2O in aqueous solution.

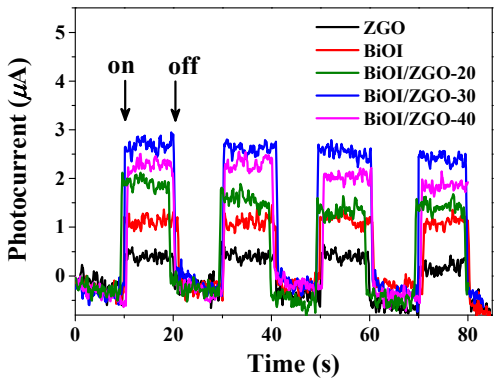

Figure 11. Transient photocurrent response of BiOI, Zn_2GeO_4, and BiOI/Zn_2GeO_4 composites.

PC and EIS measurements

The photocurrent−time measurement (PC) was developed to further illuminate the interfacial charge transfer dynamics in BiOI/Zn_2GeO_4 composite. The transient photocurrent value represents the charge collection efficiency. The higher the transient photocurrent value is, the higher the electrons-holes separation efficiency is, which is conducive to the photocatalytic reaction [40]. Figure 11 displays the photocurrent−time curves of BiOI, Zn_2GeO_4, and BiOI/Zn_2GeO_4 composites with intermittent visible light irradiation. The BiOI/ZGO-30 composite presents a higher photocurrent intensity.

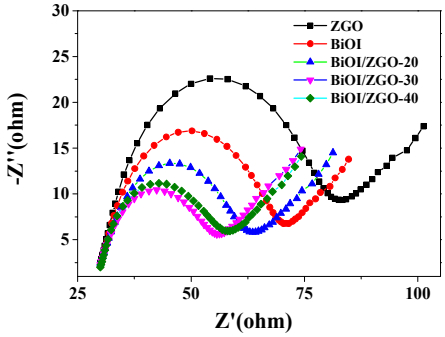

Figure 12. Nyquist plots for BiOI, Zn_2GeO_4, and BiOI/Zn_2GeO_4 composites.

The typical electrochemical impedance spectra (EIS) of BiOI, Zn_2GeO_4, and BiOI/Zn_2GeO_4 composites are presented in Figure 12. As we can see, the semicircle of BiOI/ZGO-30 in the Nyquist plots is smaller than that of BiOI, Zn_2GeO_4, and other BiOI/Zn_2GeO_4 composites, which demonstrates a decrement of

resistance in the interface and corresponding the charge transfer on the surface. These results implied that the formation of $BiOI/Zn_2GeO_4$ heterojunction was conduce to the suppression of charge recombination, and thereby a higher BPA degradation rate could be achieved in the photocatalytic system.

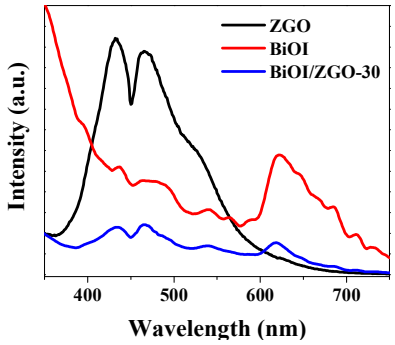

Figure 13. PL spectra of BiOI, Zn_2GeO_4 and BiOI/ZGO-30 composite.

Photoluminescence spectra

The photoluminescence (PL) spectra technology was employed to further investigate that the improvement of photo-degradation activity can be ascribed to the better photo-generated carrier separation efficiency in $BiOI/Zn_2GeO_4$ heterostructures. As shown in Figure 13, when excited by 320 nm, two strong broad emission peaks at around 432 and 467 nm are observed for Zn_2GeO_4, and that around 623 nm for BiOI. In contrast, the emission intensity from the BiOI/ZGO-30 is clearly reduced. This results suggest that the recombination of photogenerated charge carriers can be effectively inhibited. Therefore, the heterostructure of $BiOI/Zn_2GeO_4$ composite is highly favorable for separating the photo induced carriers during the photocatalytic reactions.

Roles of reactive species

To investigate the photocatalysis mechanism of BPA degradation in detail, we carried out different radicals and holes trapping experiments. In the experiments, benzoquinone (BQ) [41], isopropyl alcohol (IPA) [42], and triethanolamine (TEOA) [43] were used as the trapping agents for $\cdot O_2^-$, ·OH and h^+, respectively. Figure 14 shows the corresponding activity curve of BPA degradation after the addition of different quenchers. As we can see, after BQ (1 mg) or TEOA (0.1 g) was added, the photo-degradation efficiency was inhibited dramatically, indicating $\cdot O_2^-$ and h^+ played a major role in the process. Differently, the photo-degradation efficiency was just reduced slightly after the addition of IPA (1 mL), revealing that ·OH played a minor role on the degradation of BPA. Notably, we all know that the ·OH radicals could be generated not only from photo-generated holes but also from photo-generated electrons, and the power for photo-generated electrons to generate ·OH radicals is much weaker than that of photo-generated holes [44]. Therefore, the photo-degradation efficiency of BPA just slightly decreased in the presence of IPA, perhaps because a small amount of ·OH radicals produced by photo-generated electrons via $\cdot O_2^-$ route. In order to confirm the role of O_2 on the photo-degradation of BPA in water solution, N_2 was bubbled through the reaction system (40 mL/min) to ensure the photo-degradation process was conducted without O_2 as an electron scavenger. The apparently reduced degradation rate of BPA indicates that O_2 is to principally act as an electron trap, resulting in the production of $\cdot O_2^-$ and suppressing the recombination of electrons and holes.

It is well known that the singlet oxygen ($^1O_2$) was one of the highly reactive oxygen species via the energy or electron transfer of photo-generated hole and superoxide radical [45]. $^1O_2$ with high energy (22.5 kcal/mol) can degrade BPA directly [42]. NaN_3 is reported as an effective scavenger of $^1O_2$ [46]. Thus, NaN_3 (2 mg), acting as $^1O_2$ scavenger, was added in the photocatalytic system. The results indicated that the degradation rate obvious attenuation, implying $^1O_2$ could be generated in the system under visible light irradiation, and it also made contributions towards the BPA degradation to a certain extent.

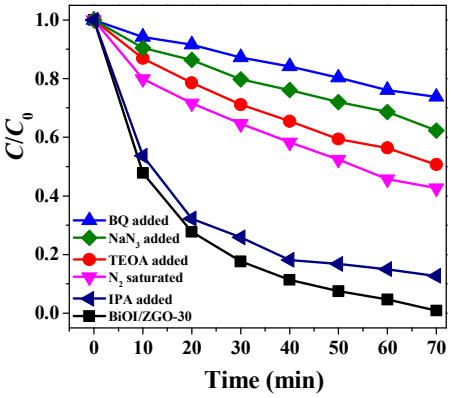

Figure 14 Effects of different scavengers on the degradation of BPA over BiOI/ZGO-30 composite under visible light irradiation.

The proposed photocatalytic mechanism

According to the band gap structure of BiOI and Zn_2GeO_4, the photoelectrochemical characterization results, and the effects of active species scavengers, a possible photocatalytic mechanism of $BiOI/Zn_2GeO_4$ photocatalyst was proposed and illustrated in **Scheme 1**. BiOI is a p-type semiconductor whose Fermi level is located close to the valence band, whereas Zn_2GeO_4 is a typical n-type semiconductor whose Fermi energy level lies close to conduction band. The p-type BiOI and n-type Zn_2GeO_4 could form the p-n heterojunction, rendering the rise of Fermi level and whole energy band of BiOI while the descent of those of Zn_2GeO_4, and the electrons diffuse from n-Zn_2GeO_4 into p-BiOI, resulting in an accumulation of negative charges in the p-BiOI region near the junction; holes diffuse from the p-BiOI region to the n-Zn_2GeO_4 region, creating a positive section in the n-Zn_2GeO_4 region in the vicinity of the junction. When the Fermi levels of BiOI and Zn_2GeO_4 reach equilibration, where in the reformed conduction band (CB) edge of BiOI exceeds that of latter, and an internal electric field directed from n-Zn_2GeO_4 to p-BiOI is simultaneously built to stop the charge diffusion from n-Zn_2GeO_4 into p-BiOI. So, when upon visible irradiation, the p-n junction would facilitate the effective separation and quick transportation of the photo-generated charge carriers. When the photocatalytic reaction was performed, only BiOI could be excited by visible light (λ > 420nm), the electron-hole pairs would be photogenerated within BiOI. Subsequently, the photo-generated electrons rapidly transferred to Zn_2GeO_4 due to the internal electric fields. The generated electrons (e^-) contacted

with O_2 to produce $\cdot O_2^-$ radical. Meanwhile, the photo-induced holes (h^+) with strong oxidation ability retained in the surface of BiOI, which could directly oxidized adsorbed BPA. Therefore, the BiOI/Zn_2GeO_4 heterostructure exhibited preferable photo-degradation activities compare with single component on the decomposition of BPA under visible light irradiation.

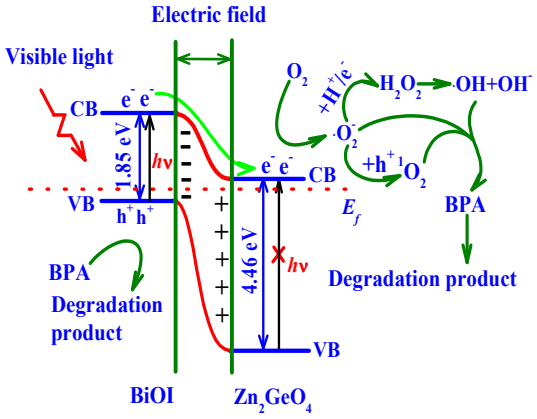

Scheme 1. Photocatalytic degradation mechanism of BPA over BiOI/Zn_2GeO_4 composites under visible light (λ > 420 nm) irradiation.

Conclusions

The BiOI/Zn_2GeO_4 composites are synthesized via a simple chemical bath approach. The BiOI/Zn_2GeO_4 heterostructures exhibited much higher photocatalytic activity for the degradation of BPA compared to single Zn_2GeO_4 and BiOI. The study results indicate that the enhancement of photocatalytic performance mainly ascribed to the strong sensitization of BiOI to Zn_2GeO_4 broadened the photoabsorption of Zn_2GeO_4, which ensured that enough photogenerated electron–hole pairs could be generated. Moreover, the p–n heterojunction structure of BiOI/Zn_2GeO_4 composite facilitated the efficient separation of photogenerated electron–hole pairs, greatly promoting the photocatalytic efficiency of Zn_2GeO_4. Furthermore, the photocatalysts exhibit excellent mineralization capacity of BPA and reliable stability, suggesting a promising prospect for the photocatalytic degradation of environmental organic pollutants in practical application.

Acknowledgment

This work was financially supported by the National Natural Science Foundation of China (No. 21175057, 21375047, and 21377046), the Natural Science Foundation of Shandong Province (No. ZR2014BL017), the Science and Technology Development Plan of Shandong Province (No. 2014GSF120004), the Special Project for Independent Innovation and Achievements Transformation of Shandong Province (2014ZZCX05101), and QW thanks the Special Foundation for Taishan Scholar Professorship of Shandong Province and UJN (No. ts20130937). Scientific Research Reward Fund for Excellent Young and Middle-Aged Scientists of Shandong Province (No. BS2012HZ001), and Scientific Research Foundation for Doctors of University of Jinan (No. XBS1037 and XKY1321).

References

1 M. Auriol, Y. FilaliMeknassi, R. D. Tyagi, C. D. Adams, R. Y. Surampalli, Process Biochem. 41 (2006) 525–539.
2 J. H. Kang, D. Aasi, Y. Katayama, Crit. Rev. Toxicol. 2007, **37**, 607.
3 E. M. Rodríguezа, G. Fernández, N. Klamerth, M. I. Maldonado, P. M. Álvarez, S. Malato, Appl. Catal., B 2010, **95**, 22.
4 D. Zalko, C. Jacques, H. Duplan, S. Bruel, E. Perdu, Chemosphere 2011, **82**, 424.
5 C. Wang, H. Zhang, F. Li, L. Zhu, Environ. Sci. Technol. 2010, **44**, 6843.
6 C. D. Robinson, E. Brown, J. A. Craft, I. M. Davies, C. F. Moffat, D. Pirie, F. Robertson, R. M Stagg, S. Struthers, Aquat. Toxicol. 2003, 62, 119.
7 C. A. Staples, P. B. Dorn, G. M. Klecka, S. T. O'Block, L. R. Harris, Chemosphere 1998, **36**, 2149.
8 G. Levy, I. Lutz, A. Krüger, W. Kloas, Environ. Res. 2004, **94**, 102.
9 B. Pan, D. H. Lin, H. Mashayekhi, B. S. Xing, Environ. Sci. Technol. 2008, **42**, 5480.
10 Y. H. Cui, X. Y. Li, and G. H. Chen, Water Res. 2009, **43**, 1968.
11 T. Hirooka, H. Nagase, K. Uchida, Y. Hiroshige, Y. Ehara, J. i. Nishikawa, T. Nishihara, K. Miyamoto, Z. Hirata, Environ. Toxicol. Chem. 2005, **24**, 1896.
12 Y. T. Xie, H. B. Li, L. Wang, Q. A. Liu, Y. Shi, H. Y. Zheng, M. Zhang, Y. T. Wu, B. Lu., Water Res. 2011, **45**, 1189.
13 M. K. Yeo, M. Kang, Water Res. 2006, **40**, 1906.
14 C. S. Guo, M. Ge, L. Liu, G. D. Gao, Y. C. Feng, Y. Q. Wang, Environ. Sci. Technol. 2010, **44**, 41.
15 C. Wang, L. Zhu, M. Wei, P. Chen, G. Shan, P, Water Res. 2012, **46**, 845.
16 J. Sato, H. Kobayashi, K. Ikarashi, N. Saito, H. Nishiyama, Y. Ioue, J. Phys. Chem. B 2004, **108**, 4369.
17 J. H. Huang, K. N. Ding, Y. D. Hou, X. C. Wang, X. Z. Fu, ChemSusChem 2008, **1**, 1011.
18 J. H. Huang, X. C. Wang, Y. D. Hou, X. F. Chen, L. Wu and X. Z. Fu, Environ. Sci. Technol. 2008, **4**, 7387.
19 Q. Liu, Y. Zhou, Z. Tian, X. Chen, J. Gao, Z. G. Zou, J. Mater. Chem. 2012, 22, 2033.
20 G. H. Jiang, R. J. Wang, X. H. Wang, X. G. Xi, R. B. Hu, Y. Zhou. S. Wang, T. Wang, W. X. Chen, ACS Appl. Mater. Interfaces 2012, **4**, 4440.
21 K. Rajeshwar, N. R. de Tacconi, C. R. Chenthamarakshan, Chem. Mater. 2001, **13**, 2765.
22 H. F. Cheng, B. B. Huang, Y. Dai, Nanoscale, 2014, 6, 2009.
23 H. F. Cheng, W. J. Wang, B. B. Huang, Z. Y. Wang, J. Zhan, X. Y. Qin, X. Y. Zhang, Y. Dai, J. Mater. Chem. A, 2013, 1, 7131.
24 X. Zhang, L. Z. Zhang, T. F. Xie, D. J. Wang, J. Phys. Chem. C 2009, **113**,7371.
25 J. Jiang, X. Zhang, P. Sun, L. Zhang, J. Phys. Chem. C 2011, **115**, 20555.
26 K. H. Reddy, S. Martha, K. M. Parida, Inorg. Chem. 2013, 52, 6390.
27 Y. Y. Li, J. S. Wang, H. C. Yao, L. Y. Dang, Z. J. Li, Catal. Commun. 2011, **12**, 660.
28 Q. Liu, Y. Zhou, J. H. Kou, X. Y. Chen, Z. P. Tian, J. Gao, S. H. Yan, Z. G. Zou, J. Am. Chem. Soc. 2010, 132, **14385**.
29 S. Yin, Y. Aita, M. Komatsu, J. S. Wang, Q. Tang, T. Sato, J. Mater. Chem. 2005, 15, 674.
30 J. Cao, B. Y. Xu, B. D. Luo, H. L. Lin, S. F. Chen, Catal. Commun. 2011, **13**, 63.
31 M. Shang, W. Z. Wang, L. Zhang, S. M. Sun, L. Wang, L. Zhou, J. Phys. Chem. C 2009, **113**, 14727.
32 J. Jiang, X. Zhang, P. B. Sun, L. Z. Zhang, J. Phys. Chem. C 2011, **115**, 20555.
33 J. Liu, G. K. Zhang, Cryst. Eng. Comm. 2013, **15**, 382.
34 Y. Y. Li, J. S. Wang, H. C. Yao, L. Y. Dang, Z. J. Li, J. Mol. Catal. A: Chem. 2011, **334**, 116.
35 H. M. Luo, A. H. Mueller, T. M. McCleskey, A. K. Burrell, E. Bauer, Q. X. Jia, J. Phys. Chem. C 2008, **112**, 6099.
36 J. H. Huang, X. C. Wang, Y. D. Hou, X. F. Chen, L. Wu, X. Z. Fu, Environ. Sci. Technol. 2008, **42**, 7387.

37 J. Cao, B. Y. Xu, H. L. Lin, B. D. Luo, S. F. Chen, Chem. Eng. J. 2012, **185**, 91.
38 Y. Xu, M. A. A. Schoonen, Am. Mineral. 2000 85, 543.
39 R. G. Pearson, Inorg. Chem. 1988, **27**, 734.
40 Y. He, J. Cai, T. Li, Y. Wu, Y. Yi, M. Luo, L. Zhao, Ind. Eng. Chem. Res. 2012, **51**, 14729.
41 M. C. Yin, Z. S. Li, J. H. Kou, Z. G. Zou, Environ. Sci. Technol. 2009,**43**, 8361.
42 L. S. Zhang, K. H. Wong, H. Y. Yip, C. Hu, J. C. Yu, C. Y. Chan, P. K. Wong, Environ. Sci. Technol. 2010 **44**, 1392.
43 Y. Y. Li, J. S. Wang, B. Liu, L. Y. Dang, H. C. Yao, Z. J. Li, Chem. Phys. Lett. 2011 **508**, 102.
44 L. Zhang, W. Z. Wang, S. M. Sun, Y. Y. Sun, E. P. Gao, Z. J. Zhang, Appl. Catal., B 2014,**148–149**, 164.
45 D. Zhang, R. Qiu, L. Song, B. Eric, Y. Mo, X. Huang, J. Hazard. Mater. 2009,**163**, 843.
46 J. W. Ng, X. P. Wang, D. D. Sun, Appl. Catal., B 2011, **110**, 260.